

基于回音壁模式的空芯光纤光流控DNA传感器

张洪鑫, 李雪刚^{**}, 周雪, 张亚男, 赵勇^{*}

东北大学信息科学与工程学院, 辽宁 沈阳 110819

摘要 针对原位DNA传感的测量需求,提出了一种基于空芯光纤回音壁模式(WGM)的光流控光纤传感器。从仿真和实验两个方面对提出的DNA传感器进行探究。通过仿真探究得到锥形光纤的尺寸、空芯光纤谐振腔的厚度以及锥形光纤和空芯光纤谐振腔的耦合间距对WGM的作用规律,在仿真规律的指导下设计和完成实验。实验结果表明,减小谐振腔的厚度可以提高传感器灵敏度,谐振腔厚度为2 μm时的折射率灵敏度可达206 nm/RIU,是厚度为4.5 μm谐振腔的灵敏度的1.4倍,满足由于DNA分子杂交而在光纤表面产生的局部折射率变化的检测灵敏度要求。通过将探针DNA固定在空芯光纤谐振腔的微流通道,可以实现互补DNA的浓度梯度检测。所提出的传感器的线性检测范围为10~100 nmol/L,灵敏度为0.56 pm/(nmol/L),线性度为0.994。此外,所提出的基于WGM的DNA光纤传感器具有很好的特异性,为原位DNA检测在医学诊断和预后中的应用提供基础。

关键词 医用光学; 光流控光纤传感器; 回音壁模式; 原位DNA传感

中图分类号 TN253; TH741

文献标志码 A

DOI: 10.3788/AOS231916

1 引言

目前,DNA检测已经广泛应用于医学诊断^[1]、环境监测^[2]、食品安全^[3]等各个领域。常见的DNA检测方法有电化学检测法^[4]、半导体检测法^[5]和光学检测法^[6]。电化学检测法具有精度高、实用性强^[7]的优点,但是该方法存在成本较高、程序和检测流程复杂、样品无法重复利用的缺点。半导体检测法^[8]可以通过半导体芯片实时检测反应发生时的变化,但实验操作难度大,而且该方法对实验体积要求严格。与传统的电化学检测法、半导体检测法相比,基于DNA分子杂交技术的光纤传感器检测法因其体积小、免标记、灵敏度高、选择性好等^[9-11]优点而受到广泛关注。

随着生物传感器的微型化发展,制作在少量样品中实现生物标志物检测的传感器引起了人们的极大兴趣。光流体技术将微流通道与光纤相结合,使得通入微流通道内的样品直接与传感表面相互作用,因此非常适合在极小的检测体积(μL量级)下进行生物/化学检测和分析。基于回音壁模式(WGM)的生物传感器因品质因数大^[12]、体积小^[13]、检测限低^[14]等优点,在高灵敏度和高精度生物传感领域展现了巨大的潜力。2016年Wu等^[15]将DNA链与微球WGM传感器集成在一起,用于检测Hg²⁺。为了进一步提高WGM的灵

敏度,2020年Brice等^[16]利用金纳米粒子在微球表面产生的局部表面等离子体共振来提高WGM的灵敏度。局域表面等离子体共振效应扩展了金纳米粒子的倏逝场,从而提高了基于WGM的传感器的灵敏度。但微球结构不易固定,泵送液体时容易对微球的位置产生影响,从而对实验结果产生干扰。此外,不具备微流通道WGM传感结构直接裸露在外部,容易受到外界环境的干扰。空芯光纤(HCF)完美地克服了这两个缺点,空芯光纤在具有自然流体通道的同时也便于固定,这为高灵敏度传感提供了基础。空芯光纤微谐振器作为WGM光流体微谐振器的一种,可以通过与空芯光纤接近的锥形光纤有效地激发WGM。此外,空芯光纤上存在的大孔径气孔提供了可供液体流通的光流控通道。光纤WGM传感器具有操作方便、与外界环境隔离、样品流体连续输送等优点。微流通道^[17]还可以通过将检测目标连续供给传感器表面来加速杂交。因此将光流体技术与空芯光纤相结合的生物传感器是生物检测和相关生化应用的理想候选传感器。

基于此,本文提出了一种基于WGM的高灵敏度光纤传感器用于特定DNA分子的检测。基于固定在该传感器微流通道表面的探针DNA(pDNA)与待测的目标DNA(cDNA)的特异性结合进行分

收稿日期: 2023-12-11; 修回日期: 2024-02-19; 录用日期: 2024-02-20; 网络首发日期: 2024-03-13

基金项目: 国家自然科学基金(62373088, 62203090, U22A2021)、广东省基础与应用研究基金(2022A1515220086)、辽宁省自然科学基金(2023-MS-076)、中国科协青年托举人才项目(2022QNRC001)

通信作者: *zhaoyong@ise.neu.edu.cn; **lixuegang@ise.neu.edu.cn

析,实现对 cDNA 的浓度梯度检测。实验结果表明该传感器的线性检测范围为 10~100 nmol/L,灵敏度为 0.56 pm/(nmol/L),这意味着该传感器可以对浓度的微小变化做出反应,可以用于高灵敏度的特异性检测。此外,该传感器的响应具有较高的线性度($R^2=0.994$)。本文所提出的传感器具有灵敏度高、稳定性好、特异性好等优点,可以很好地应用于 DNA 的检测,为基于 WGM 的光纤生物传感器的应用开辟了新的前景,也拓展了光纤 DNA 传感器的应用领域。

2 结构与原理

锥形光纤耦合空芯光纤的传感结构示意图如图 1 所示。当输入光进入传感结构的锥形区域时,产生倏逝场。当锥形光纤与空芯光纤距离较近时,锥形光纤的部分倏逝场耦合到空芯光纤中,耦合进入空芯光纤的光在谐振腔内以全反射形式传输,并在表面处产生倏逝场,实现对内部微流通道的监测。

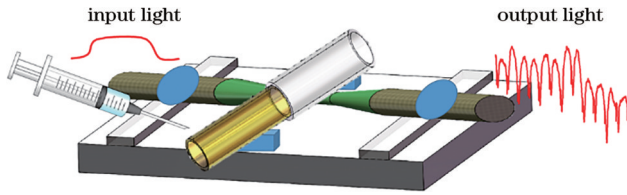


图 1 封装后的传感结构示意图

Fig. 1 Schematic diagram of packaged sensor

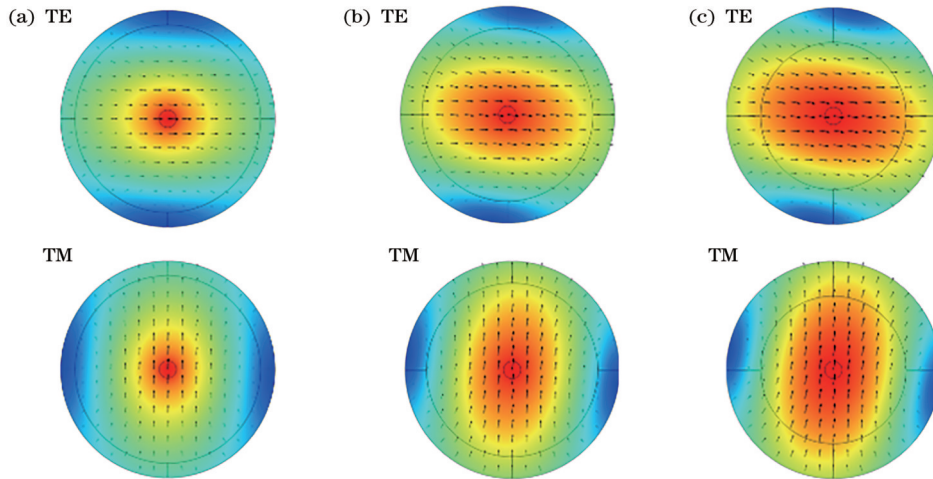


图 2 不同锥形光纤直径下的电场分布。(a) 2.4 μm ; (b) 1.6 μm ; (c) 1.2 μm

Fig. 2 Electric field distributions under different tapered fiber diameters. (a) 2.4 μm ; (b) 1.6 μm ; (c) 1.2 μm

3.2 微腔尺寸对回音壁模式的影响

由式(1)可知,微腔的直径发生改变时,环形波导发生改变,电场也会随之改变。通过仿真探究不同的微腔尺寸对于 WGM 模式的影响,观察不同直径情况下的谐振腔电场分布。

如图 3 所示,随着谐振腔厚度不断减小,分布在谐振腔内的电场增强,回音壁模式效果更明显。从仿真结果可以看出,谐振腔厚度为 2 μm 时模场可达到最

基于 WGM 原理的数学方法^[18]描述为

$$2\pi R n_{\text{eff}} = m\lambda, \quad (1)$$

式中: n_{eff} 为有效折射率; R 为空芯光纤的半径; m 为 WGM 角动量(整数)。谐振条件满足式(1)的光耦合到空芯光纤微谐振器中,产生 WGM,输出光谱如图 1 所示。

当不同折射率的溶液通入空芯光纤的微流通道时,微腔的有效折射率 n_{eff} 会发生变化,导致 WGM 的输出光谱发生偏移,实现对外部环境的检测。本文通过表面功能化处理将 pDNA 固定在微流通道表面。cDNA 与 pDNA 的特异性结合导致 n_{eff} 的变化,造成 WGM 光谱的偏移,进而实现对 cDNA 的检测。

3 仿真实验

3.1 锥形光纤直径对回音壁模式的影响

本文利用 Comsol 软件来模拟锥形光纤直径不断减小时电场的矢量分布,仿真结果如图 2 所示。光在锥形光纤过渡区域传输时,随着锥区直径的逐渐减小,锥形光纤中传输的模场能量逐渐从锥形光纤泄漏到外部环境中。泄漏到外部环境中的能量越强,则倏逝场越强,越有利于谐振腔 WGM 的激发。从仿真结果可以看出,锥形光纤的直径为 1.2 μm 时倏逝场强度达到最高。当锥形光纤直径减小时,结构会变得脆弱,为了保证结构的稳定性和鲁棒性,选择直径为 1.2 μm 的锥形光纤进行实验。

强,由此产生的倏逝场也会更强。但当谐振腔较薄时,微流泵输送液体产生的压力会导致微流通道破裂。为保证结构的稳定性,选择厚度为 2 μm 的谐振腔进行实验。

3.3 耦合间距对回音壁模式的影响

耦合间距对谐振腔的特性有一定的影响,本文仿真分析了耦合间距为 2.0 μm 、1 μm 、0.6 μm 时谐振腔的电场分布,如图 4 所示。

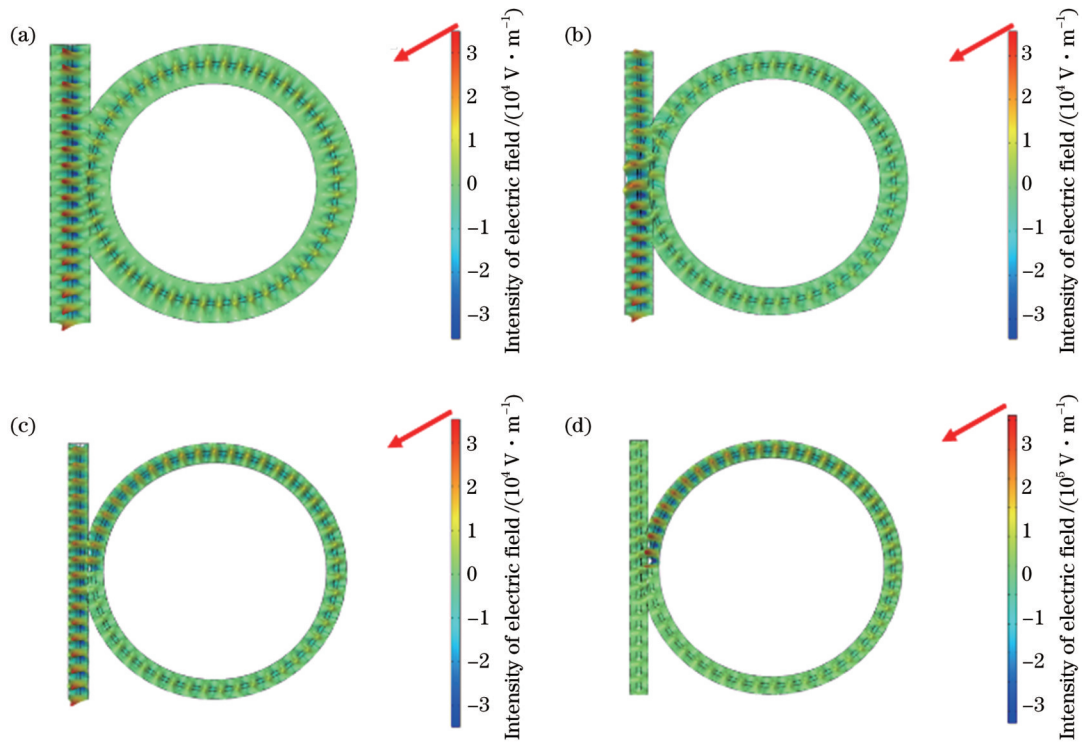


图 3 不同壁厚下谐振腔的电场分布情况。(a)厚度为 $10\ \mu\text{m}$; (b)厚度为 $6.5\ \mu\text{m}$; (c)厚度为 $2.5\ \mu\text{m}$; (d)厚度为 $2\ \mu\text{m}$

Fig. 3 Electric field distributions of resonator under different wall thicknesses. (a) Thickness is $10\ \mu\text{m}$; (b) thickness is $6.5\ \mu\text{m}$; (c) thickness is $2.5\ \mu\text{m}$; (d) thickness is $2\ \mu\text{m}$

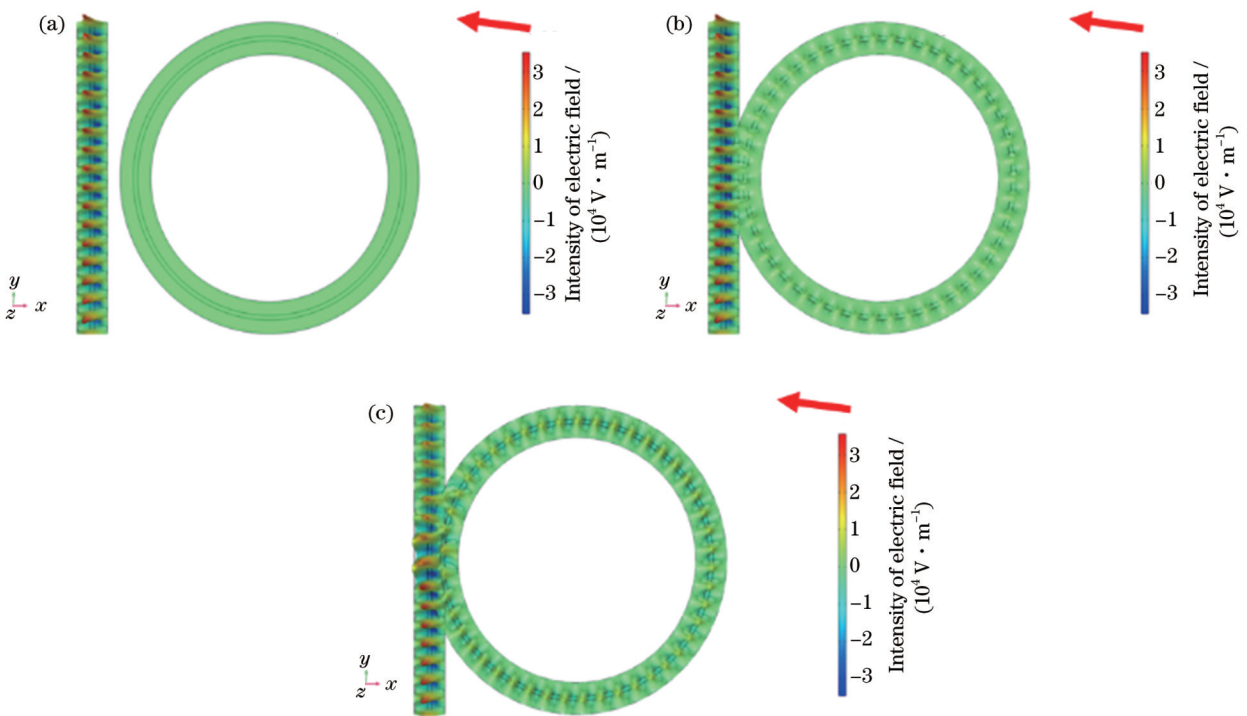


图 4 不同耦合间距下的电场分布。(a)耦合间距为 $2\ \mu\text{m}$; (b)耦合间距为 $1\ \mu\text{m}$; (c)耦合间距为 $0.6\ \mu\text{m}$

Fig. 4 Electric field distributions under different coupling distances. (a) Coupling distance is $2\ \mu\text{m}$; (b) coupling distance is $1\ \mu\text{m}$; (c) coupling distance is $0.6\ \mu\text{m}$

通过对这些电场分布图进行分析,发现当耦合间距过大时,无法产生 WGM 现象。随着耦合间距的不断减小,WGM 越来越明显。耦合间距过小会造成谐

振腔与锥形光纤的直接接触,进而造成锥形光纤断裂。因此,后续实验中利用三维调整架将耦合间距调整为 $0.6\ \mu\text{m}$ 。

4 实验验证和结果结论

4.1 探头制备及实验系统搭建

实验结构的制备过程如下。首先利用光纤拉锥机 (IPCS-5000) 将单模光纤拉制成锥区长度为 10 mm、锥区直径为 $1.2 \mu\text{m}$ 的锥形光纤。将 3 cm 长的空芯光纤垂直放置在锥形光纤锥区上方, 利用三维调整架调节锥形光纤与空芯光纤之间的耦合距离, 则特定的耦合间距处产生 WGM 现象。为保证锥形光纤和空芯光纤的稳定耦合, 采用一种简单的封装方式, 将长为 1 cm、宽为 0.3 cm、厚为 0.2 cm 的玻璃片放在空芯光纤两侧, 将 UV 黏合剂滴在两块小玻璃片上方和两侧, 利用紫外灯固化 30 s, 完成空芯光纤的固定, 进而保证后续实验中耦合间距不发生改变。

整个实验系统是由光学测量装置和流体供应装置两部分组成, 如图 5 所示。使用微流泵 (LONGER COMPANY, L100-1S-1) 将溶液泵入空芯光纤。保持传感器与微流泵输出端在同一水平线上。光学装置包括光源范围为 1520~1610 nm 的宽带光源 (CONQUER KG-ASE8097) 和光谱仪 (OSA, Yokogawa AQ6370D)。当输入光通过锥形光纤区域时, 锥形区域产生倏逝场, 倏逝场部分耦合到锥形光纤上方的空芯光纤中并激发 WGM, 通过 WGM 光谱的变化实现传感。

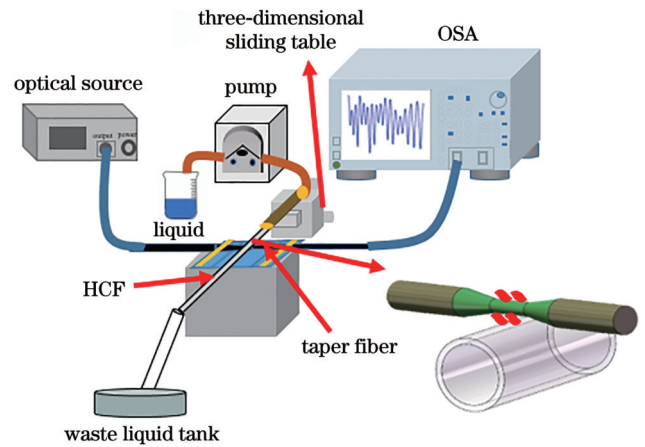


图 5 实验装置示意图

Fig. 5 Schematic diagram of experimental device

4.2 传感器的光学特性

传感器的一个重要特性是具备很高的灵敏度。为了便于观察, 将不同浓度氯化钠溶液的光谱沿纵轴交错排列。

通过 3.2 节的仿真可知, 空芯光纤管壁较厚时, 也可以产生 WGM 现象。但是谐振腔内的电场强度较低, 在结果上表现为折射率灵敏度低。图 6(a) 所示为壁厚为 $4.5 \mu\text{m}$ 的传感器的光谱图。折射率灵敏度拟合曲线如图 6(b) 所示, 结果为 $141 \text{ nm}/\text{RIU}$ 。

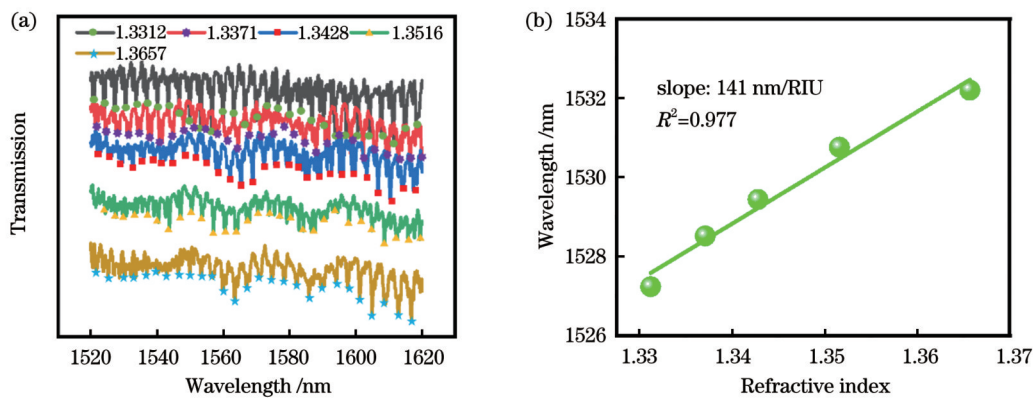


图 6 管壁厚度为 $4.5 \mu\text{m}$ 的 WGM 折射率光谱图及灵敏度拟合曲线。(a) 折射率光谱图; (b) 灵敏度拟合曲线

Fig. 6 Refractive index spectra and sensitivity fitting curve of WGM with $4.5 \mu\text{m}$ thickness tube. (a) Refractive index spectra; (b) sensitivity fitting curve

为了进一步提高传感器的灵敏度, 使用质量分数为 40% 的氢氟酸对空芯光纤谐振腔进行腐蚀。经过氢氟酸蚀刻处理后, 谐振腔的壁厚为 $2 \mu\text{m}$, 利用腐蚀后的空芯光纤制备的传感器进行折射率传感实验, 光谱如图 7(a) 所示。腐蚀后的传感器的折射率灵敏度为 $206 \text{ nm}/\text{RIU}$, 相较于 $4.5 \mu\text{m}$ 的谐振腔有了显著的提高, 灵敏度拟合曲线如图 7(b) 所示。

4.3 DNA 传感实验

微流通道的功能化过程如图 8 所示。利用微流泵以 $200 \mu\text{L}/\text{min}$ 的速度向空芯光纤内通入超纯水, 清洗

传感器探头 10 min。清洗完传感区域后, 以 $100 \mu\text{L}/\text{min}$ 的速度向微流通道内通入 $1 \text{ mol}/\text{L}$ 的 NaOH 溶液 50 min, 以使微流通道内表面带—OH 基团^[19]。接着, 以 $100 \mu\text{L}/\text{min}$ 的速度向微流通道内通入空气 60 min, 吹出残余的 NaOH 溶液以实现微流通道内表面的干燥。干燥后再以 $50 \mu\text{L}/\text{min}$ 的速度向微流通道内注入质量分数为 10% 的 3-氨基丙基三乙氧基硅烷溶液 15 min, 在微流通道的内表面产生—NH₃^[20]。处理后再次利用超纯水洗涤, 以去除非共价结合的硅烷化合物。

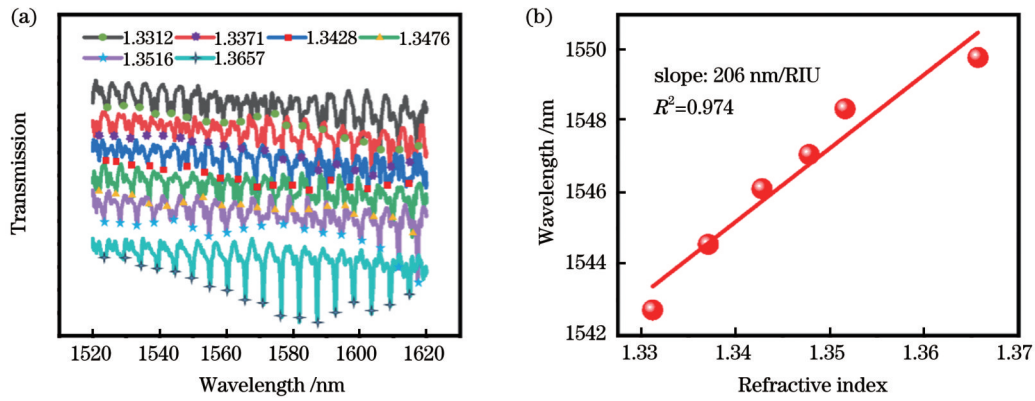


图7 管壁厚度为2 μm 的WGM折射率光谱图及灵敏度拟合曲线。(a)折射率光谱图;(b)灵敏度拟合曲线

Fig. 7 Refractive index spectra and sensitivity fitting curve of WGM with 2 μm thickness tube. (a) Refractive index spectra; (b) sensitivity fitting curve

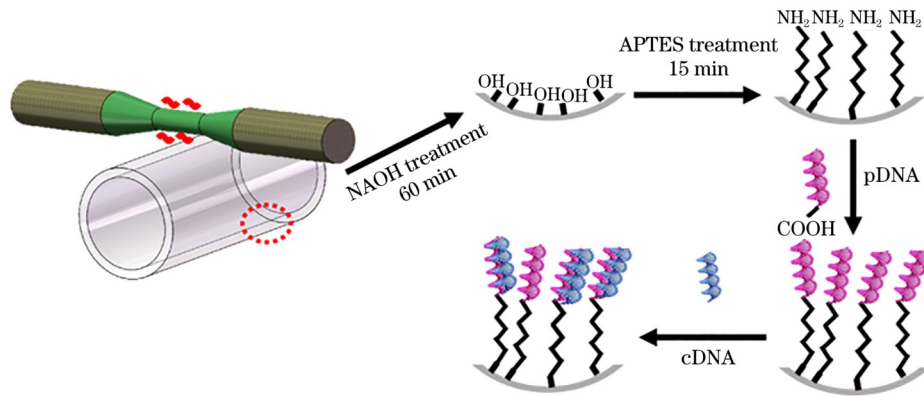


图8 光流控WGM谐振器的功能化方法

Fig. 8 Functionalization method of WGM optofluidic resonator

以50 $\mu\text{L}/\text{min}$ 的速度向微流通道内通入浓度为1 $\mu\text{mol}/\text{L}$ 的pDNA溶液20 min以固定pDNA。pDNA上有一COOH,可以通过氨基和羧基结合的方式将pDNA固定在微流通道,此时完成pDNA的修饰,用于cDNA的特异性检测。

利用上述的步骤对传感器进行功能化,在每一步光谱稳定后记录光谱,并用不同浓度梯度的cDNA溶液对传感器的性能进行测试,光谱如图9(a)所示。cDNA被微流通道表面修饰的pDNA连续捕获,会导致微流通道表面的局部环境折射率增加,波谷发生红移,红移程度与cDNA的浓度有关。图9(b)显示了同一个WGM波谷对cDNA溶液从低浓度到高浓度的响应光谱。红移程度与cDNA浓度的关系如图9(c)所示,10 nmol/L、50 nmol/L、100 nmol/L、200 nmol/L、1 $\mu\text{mol}/\text{L}$ 浓度的cDNA的红移量分别为50 pm、70 pm、100 pm、110 pm和110 pm。当cDNA的浓度超过200 nmol/L时,光谱不再发生红移,表明了微流通道的pDNA已经被完全结合,传感器达到了饱和状态。实验结果表明WGM光谱的移动量随cDNA浓度的升高而增大,且位移程度和cDNA浓度之间的关系是线性的。本文所提出的传感器的线性检测

范围为10~100 nmol/L,特异性检测的灵敏度为0.56 pm/(nmol/L)。

利用与pDNA互补的cDNA以及非互补的tDNA进行了传感器的特异性实验,光谱如图10(a)所示。从图10(b)的波长偏移中可以看出,互补cDNA移动量为52 pm,远大于相同浓度的非互补tDNA的4 pm,这证明本文提出的传感器具有很好的特异性。

传感器的稳定性是衡量传感器性能的另一个重要指标。在进行tDNA的检测后,对传感器进行了40 min的稳定性测试,每10 min记录一次光谱。监测一个WGM的谷值,将获得的5组数据取平均值作为基准值。经计算可得,传感器的标准偏差为6.2 pm。从图10(c)中可以看出:随着时间的推移,传感器的稳定性良好。图10(c)中 σ 为标准差。

为了评估所提出的传感器的传感性能,从结构、检测范围以及传感器的灵敏度出发将其与现有的基于WGM的DNA传感器进行比较,并在表1中列出。与其他不同结构的传感器相比,本文提出的方法实现传感器灵敏度的显著提升,利用微流通道可实现光流控检测。此外,本文方法在节省试剂等方面具有更加独特的优势。

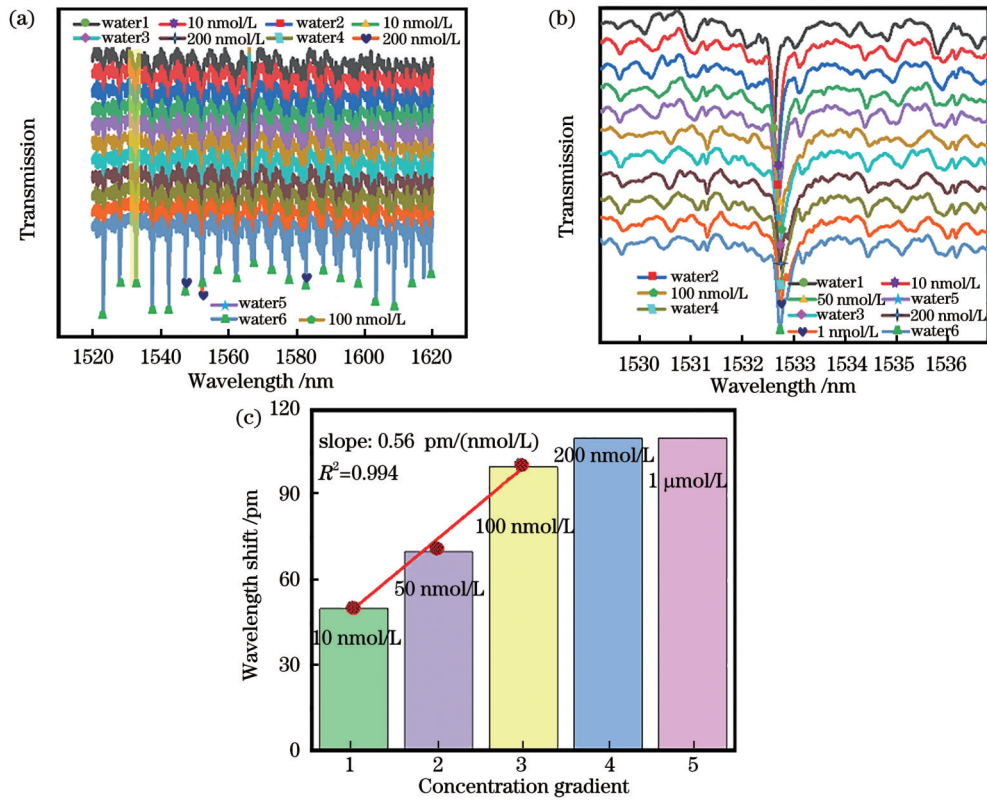


图 9 传感器 DNA 浓度梯度检测实验。(a)不同浓度梯度下的 WGM 光谱图;(b)传感监测的局域光谱图;(c)不同浓度下的波长移动图
Fig. 9 DNA concentration gradient detection experiment of the proposed sensor. (a) WGM spectra under different concentration gradients; (b) localized spectra monitored by sensing; (c) wavelength shift diagram at different concentrations

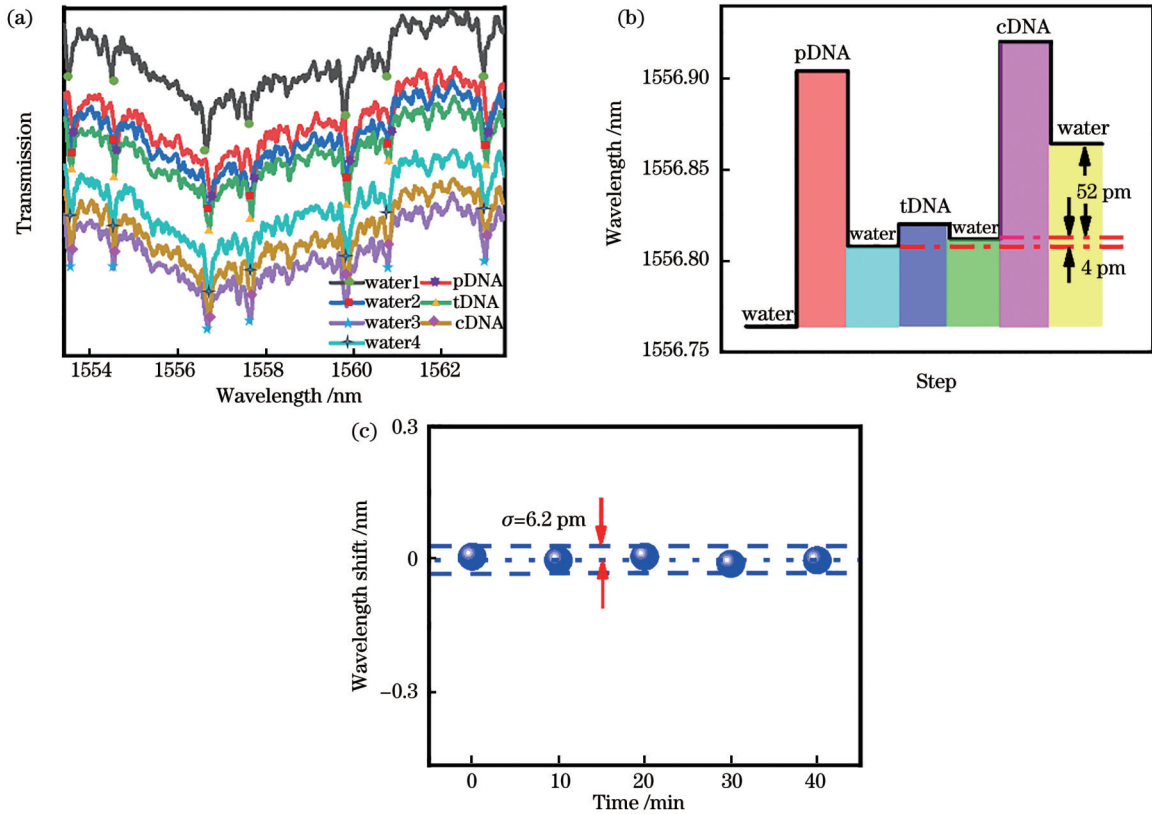


图 10 传感器的传感性能实验。(a)传感器的特异性实验;(b)不同步骤下的光谱移动量图;(c)传感器的稳定性实验
Fig. 10 Sensing performance experiments of the proposed sensor. (a) Specificity experiment of sensor; (b) spectral shift diagram under different steps; (c) stability experiment of sensor

表 1 采用 WGM 测量 DNA 分子的传感器性能比较
Table 1 Comparison of performance of DNA molecule sensors using WGM

Structure	Range /(nmol/L)	Sensitivity /(nm/RIU)	Optofluidic	Reference
Microsphere	20	13.60	No	Ref. [21]
Microring	0.5–500	37.10	Yes	Ref. [22]
Double-arc microcapillary	0.1–10	5.36	No	Ref. [23]
Microtubule	10–100	206.00	Yes	Our work

5 结 论

本文提出了一种基于空芯光纤的 WGM 光流控传感器,实现了对 DNA 分子的高灵敏、高特异性的检测。通过减小空芯光纤谐振腔的厚度提高传感器的灵敏度。实验结果表明,传感器可以将 pDNA 固定在谐振腔的微流通道内作为捕获 cDNA 的探针,实现 cDNA 的定量检测。实验结果表明,在 25 °C 温度下,本文提出的传感器能够检测不同浓度梯度下的特定 DNA 片段,线性检测范围为 10~100 nmol/L,灵敏度为 0.56 pm/(nmol/L)。总之,这项工作有很大的潜力扩展到 DNA 传感在医学诊断和预后中的应用,为实现集成化和多路复用提供基础。

参 考 文 献

- [1] Li F, Li X G, Zhou X, et al. Plug-in label-free optical fiber DNA hybridization sensor based on C-type fiber Vernier effect[J]. *Sensors and Actuators B: Chemical*, 2022, 354: 131212.
- [2] Tang Y, Gu C, Wang C, et al. Evanescent wave aptasensor for continuous and online aminoglycoside antibiotics detection based on target binding facilitated fluorescence quenching[J]. *Biosensors and Bioelectronics*, 2018, 102: 646-651.
- [3] Mahgoub Y A, Shawky E, Eldakak M, et al. Plant DNA barcoding and metabolomics for comprehensive discrimination of German Chamomile from its poisonous adulterants for food safety[J]. *Food Control*, 2022, 136: 108840.
- [4] Hai X, Li Y F, Zhu C Z, et al. DNA-based label-free electrochemical biosensors: from principles to applications[J]. *TrAC Trends in Analytical Chemistry*, 2020, 133: 116098.
- [5] 孙云, 蒋涛, 马定远, 等. 新一代半导体测序技术检测甲基丙二酸血症 MMAA 基因突变[J]. *中华医学遗传学杂志*, 2015, 32(1): 56-59.
Sun Y, Jiang T, Ma D Y, et al. Detection of pathogenic mutations for methylmalonic acidemia using new-generation semiconductor targeted sequencing[J]. *Chinese Journal of Medical Genetics*, 2015, 32(1): 56-59.
- [6] Pereira D, Bierlich J, Kobelke J, et al. Optical fiber sensor for monitoring the evaporation of ethanol-water mixtures[J]. *Sensors*, 2022, 22(15): 5498.
- [7] 熊庭超, 殷延益, 陆丹华, 等. 激光重熔/电化学沉积交互处理铜涂层的微观组织及机理研究[J]. *中国激光*, 2023, 50(4): 0402007.
Xiong T C, Yin Y Y, Lu D H, et al. Microstructure and mechanism of copper layer processed with laser remelting and electrochemical deposition interaction process[J]. *Chinese Journal of Lasers*, 2023, 50(4): 0402007.
- [8] 林涛, 解佳男, 穆妍, 等. Ge/Si₂Ge_{1-x} 衬底 620 nm 半导体激光器的特性[J]. *激光与光电子学进展*, 2022, 59(19): 1914003.
Lin T, Xie J N, Mu Y, et al. Properties of 620 nm semiconductor lasers with Ge/Si₂Ge_{1-x} substrate[J]. *Laser & Optoelectronics Progress*, 2022, 59(19): 1914003.
- [9] Li X G, Chen N, Zhou X, et al. *In-situ* DNA detection with an interferometric-type optical sensor based on tapered exposed core microstructured optical fiber[J]. *Sensors and Actuators B: Chemical*, 2022, 351: 130942.
- [10] 张诚, 马雪慧, 赵军发, 等. 基于虚拟游标增敏的法布里-珀罗温度传感器[J]. *中国激光*, 2023, 50(13): 1310002.
Zhang C, Ma X H, Zhao J F, et al. Fabry-Perot temperature sensor based on virtual vernier sensitization[J]. *Chinese Journal of Lasers*, 2023, 50(13): 1310002.
- [11] Zheng W L, Han B, Zhang Y N, et al. An in-fiber sensor for simultaneous measurement of cholesterol concentration and temperature based on SPR and MMI[J]. *Analytica Chimica Acta*, 2024, 1287: 342043.
- [12] Hammer K J, Buma T. Microsphere resonator for optoacoustic detection of high frequency ultrasound[C]//2014 IEEE International Ultrasonics Symposium, September 3–6, 2014, Chicago, IL, USA. New York: IEEE Press, 2014: 955-958.
- [13] Wang Y Y, Zeng S W, Humbert G, et al. Microfluidic whispering gallery mode optical sensors for biological applications[J]. *Laser & Photonics Reviews*, 2020, 14(12): 2000135.
- [14] Niu P P, Jiang J F, Liu K, et al. Fiber-integrated WGM optofluidic chip enhanced by microwave photonic analyzer for cardiac biomarker detection with ultra-high resolution[J]. *Biosensors and Bioelectronics*, 2022, 208: 114238.
- [15] Wu F C, Wu Y Q, Niu Z W, et al. Integrating a DNA strand displacement reaction with a whispering gallery mode sensor for label-free mercury (II) ion detection[J]. *Sensors*, 2016, 16(8): 1197.
- [16] Brice I, Grundsteins K, Atvars A, et al. Whispering gallery mode resonator and glucose oxidase based glucose biosensor[J]. *Sensors and Actuators B: Chemical*, 2020, 318: 128004.
- [17] 苑婷婷, 张晓彤, 杨兴华, 等. 微流光纤传感器:从功能集成到功能设计[J]. *激光与光电子学进展*, 2024, 61(1): 0106004.
Yuan T T, Zhang X T, Yang X H, et al. Microfluidic fiber optic sensors: from functional integration to functional design[J]. *Laser & Optoelectronics Progress*, 2024, 61(1): 0106004.
- [18] Ahn I H, Yeo S J, Jung K, et al. A multi-functional highly efficient upconversion luminescent film with an array of dielectric microbeads decorated with metal nanoparticles[J]. *Advanced Functional Materials*, 2020, 30(13): 1909445.
- [19] Mohsin A Z, Sukor R, Mustapha-Kamil Y, et al. Sensitive detection of goat α_1 -casein using tapered optical fiber sensor[J]. *IEEE Journal of Selected Topics in Quantum Electronics*, 2021, 27(4): 5600507.
- [20] Shen C Y, Chen X M, Huang Z L, et al. High sensitivity and fast response optical fiber nucleic acid sensor[J]. *Optics & Laser Technology*, 2022, 154: 108271.
- [21] Zhou X, Wang S K, Li X G, et al. Whispering gallery mode microresonator sensor integrated in exposed core fiber for label-free DNA hybridization detection[J]. *Journal of Lightwave Technology*, 2023, 41(13): 4502-4508.
- [22] Suter J D, White I M, Zhu H Y, et al. Label-free quantitative DNA detection using the liquid core optical ring resonator[J].

Biosensors and Bioelectronics, 2008, 23(7): 1003-1009.

[23] Zhang S, Lu Y, Liang Z W, et al. A high-Q, double-arc microcapillary biosensor for DNA detection with high speed,

low sample volume[C]//Asia Communications and Photonics Conference 2021, October 24-27, 2021, Shanghai. Washington, DC: Optica Publishing Group, 2021: M5G.5.

Hollow-Core Optical Fiber Optofluidic DNA Sensor Based on Whispering Gallery Mode

Zhang Hongxin, Li Xuegang^{**}, Zhou Xue, Zhang Yanan, Zhao Yong^{*}

College of Information Science and Engineering, Northeastern University, Shenyang 110819, Liaoning, China

Abstract

Objective The specific detection of DNA sequences plays a vital role in disease diagnosis, drug development, environmental protection, and other fields. Common DNA detection methods include electrochemical detection, semiconductor detection, and optical detection. Although the electrochemical detection method features high precision and strong practicability, it has the disadvantages of high cost and complicated detection processes. Semiconductor detection methods can detect reaction changes in real time, but the experimental operation is difficult and has strict requirements for experimental volume. Optical fiber biosensors based on the whispering gallery mode (WGM) effect have been extensively studied due to their small size, high detection accuracy, and fast response. For the measurement requirements of *in-situ* DNA sensing, we propose an optical fiber optofluidic sensor based on hollow-core fiber WGM.

Methods The proposed sensor is prepared by coupling a tapered optical fiber and a hollow-core fiber. The sensor mainly employs the evanescent field generated by the tapered optical fiber to excite the hollow-core fiber resonant cavity to generate WGM for detection. From the perspective of the sensor composition, the diameter of the tapered fiber, the thickness of the resonant cavity, and the coupling distance between the tapered fiber and the resonant cavity will all influence the experimental detection results. Meanwhile, we explore the proposed DNA sensor from both simulation and experiment aspects. By conducting simulation analysis via Comsol software, we first obtain how the above three factors affect the experimental results. The experiment is completed under the guidance of the simulation. Additionally, we adopt the hollow-core fiber as the resonant cavity and the internal air hole of the hollow-core fiber as the microfluidic channel. In the experiment, the silanization method is utilized to immobilize probe DNA (pDNA) on the surface of the resonant cavity for subsequent detection of complementary DNA (cDNA).

Results and Discussions The simulation experiments can help draw the following three conclusions. The smaller diameter of the tapered zone of the tapered fiber leads to a stronger evanescent field generated by the tapered fiber. When the thickness of the resonant cavity continues to decrease, the higher electric field in the resonant cavity brings stronger generated WGM. Under the constant diameter of the tapered fiber and thickness of the resonant cavity, the WGM phenomenon will occur when the coupling spacing between the tapered fiber and the resonant cavity is reduced to a certain distance. The experimental results show that reducing the thickness of the resonant cavity can improve the sensor sensitivity. When the thickness of the resonator is 4.5 μm , the refractive index sensitivity is 141 nm/RIU. The simulation results indicate that reducing the thickness of the resonant cavity can increase the sensor sensitivity. Meanwhile, we leverage hydrofluoric acid to corrode the thickness of the resonant cavity. When the thickness of the resonator is 2 μm , the refractive index sensitivity can reach 206 nm/RIU, 1.4 times higher than that of the resonator with a thickness of 4.5 μm . The thickness of the resonant cavity less than 2 μm is not suitable for practical experiments. The thickness of the hollow-core fiber during the preparation process is not completely uniform. When the thickness of the resonant cavity corroded by hydrofluoric acid is less than 2 μm , it is easy to corrode the thinner parts of the resonant cavity. Additionally, to achieve the introduction of the liquid to be measured, we employ a pump to transport the liquid, which will generate pressure on the resonant cavity and cause the microfluidic channel to rupture under the thin thickness. The resonant cavity with a thickness of 2 μm meets the requirements for detecting local refractive index changes that occur on the optical fiber surface due to the hybridization of DNA molecules. The specific detection of complementary DNA can be achieved by immobilizing the pDNA inside the microfluidic channel of the hollow-core fiber resonator. We prepare cDNA solutions with five concentrations of 10 nmol/L, 50 nmol/L, 100 nmol/L, 200 nmol/L, and 1 $\mu\text{mol/L}$ for concentration gradient detection.

When the concentration is 10–100 nmol/L, since the amount of pDNA on the inner surface of the resonant cavity is large enough, linear changes occur with the increasing cDNA concentration. When the concentration of cDNA is 200 nmol/L, the remaining pDNA cannot completely bind to cDNA and therefore cannot change linearly. When the concentration of cDNA continues to rise, there is no excess pDNA on the fiber surface, the sensor reaches a saturated state, and the spectrum no longer shifts. Therefore, the proposed sensor has a linear detection range of 10–100 nmol/L, a sensitivity of 0.56 pm/(nmol/L), and a linearity of 0.994, and it has sound stability and selectivity.

Conclusions In this paper, we proposed and exhibited a high-sensitivity optical fiber DNA sensor. The WGM fiber probe was fabricated by embedding a corroded hollow core fiber into the tapered fiber structure, and the WGMs could be excited through the efficient coupling between the thin hollow core fiber and the tapered fiber. WGMs in the resonator are excited by evanescent coupling using the tapered fiber with 1.2 μm waist diameter. The combination of proposed DNA and complementary DNA will increase the effective refractive index of the microtubule change, and result in transmission spectrum change finally. Studies of the DNA response sensitivity, stability, and selectivity dependence of the proposed sensor are carried out. The sensitivity achieved in our experiments was 0.56 pm/(nmol/L) in the DNA range from 10 nmol/L to 100 nmol/L. Our DNA sensor based on the WGM effect has the advantage of label-free detection, laying the foundation for the applications of *in-situ* DNA detection in medical diagnosis and prognosis.

Key words medical optics; optofluidic optical fiber sensor; whispering gallery mode; *in-situ* DNA sensing